Performance Analysis of Drone Assisted Multiple Antenna Backscatter IoT Sensor Network

Ali M. Hayajneh[1], Haitham Al-Obiedollah[1], Haythem Bany Salameh[2,3], Massimo Merenda[4], Sofyan M. Hayajneh[5], Syed Ali Raza Zaidi[6], Des. C. McLernon[7]
[1]Department of Electrical Engineering, The Hashemite University, Zarqa, Jordan
[2]College of Engineering, Al Ain University, Al Ain, UAE
[3]Telecommuniation Engineering Department, Yarmouk University, Jordan
[4]Delle Infrastrutture e dell'Energia Sostenibile (DIIES), Mediterranea University, Reggio Calabria, Italy
[5]Faculty of Computer Studies, Arab Open University, Jordan
[6]School of Electronic and Electrical Engineering, University of Leeds, Leeds, United Kingdom

***Abstract*—In this paper, we investigate the idea of drone-assisted multiple antenna ambient backscatter communication (AmBC) based internet of things (IoT) sensor network (SN). We consider a scenario where a drone is used to collect the data from distributed multiple antenna SNs at which the drone is working as an ambient power emitter and a reader. The sensor nodes passively modulate the transmitted pure carrier by implementing load impedance modulation which results in an amplitude shift keying modulation. In order to quantify the performance of the studied network, we aim to find a closed-form expression for the coverage probability for the AmBC double-Rayleigh dyadic fading channel. Our model also incorporates Line of Sight (LoS) and Non-LoS (NLoS) propagation states for accurately modeling large-scale path-loss between drone and SN. We also investigate the use of the method of the moments in finding the probability density function (PDF) for the overall fading channel by matching it to a Log-Normal distribution to ease the mathematical manipulations. Finally, numerical results are compared to Monte-Carlo simulations to verify the effectiveness of the derived system model analysis and to characterize the optimal selection of the network parameters in maximizing the coverage probability.**

***Index Terms*—Drone, Backscatter communication, Dyadic fading, IoT, Coverage probability**

I. Introduction

With the proliferation of smart connected, sensing devices and the massive IoT applications as key enablers of smart cities, there is a dire need for a more flexible platform to deliver IoT data in private, low-power, and efficient ways. These IoT applications, in essence, require an energy-efficient, low latency, high data-rate communication, and a learning paradigm to decrease the footprint of the connected devices on the network bandwidth and latency [1], [2].

In multiple applications (e.g., smart agriculture and smart cities), there is a dense deployment of smart IoT devices and this requires sophisticated models for the radio access network (RAN) and interference management. The need for dense deployment of IoT-connected devices is defined by the International Telecommunications Union (ITU) as massive Machine-Type Communications (mMTC) and this type of deployment with some characteristics of the ultra-reliable and low latency communications (URLLC) requires the adoption of more agile and responsive networks [3]. Also, the wireless infrastructure is not always available, and if it exists it adds a huge footprint on the capital and operational expenditure (CAPEX/OPEX) to secure the wireless communication.

In order to solve the needs for instant low-cost infrastructure in the interference-rich fields, drones or unmanned aerial vehicles (UAVs), due to their agile nature, can be harnessed to serve as temporary drone base stations (DBSs) or gateways and hence can serve for wide fields of mMTC kind of IoT networks [4]. This requires an intelligent trajectory, RAN utilization, and efficient resource allocation. The key feature of flying objects and the vertical design of UAV IoT networks is the desirable channel characteristics for the air to ground (A2G) link. UAVs provide better line of sight (LoS) link characteristics, and thus the quality of the network can be enhanced. However, increasing the LoS link probability can increase the co-channel interference between different locations of the network and hence an optimal localization and interference management for drones to ground is required [5]–[11].

In order to tackle the issue of the high CAPEX in the infrastructure of the dense SNs, backscatter communication, [12]–[21] presents an attractive alternative that can be deployed densely with very low cost. Backscatter radio communication does not require expensive active components such as RF oscillators, mixers, crystals, decoupling capacitors, etc. The SNs communicate with the access point (AP), also called the Reader which is presented in this article as drone readers, by modulating the ambient un-modulated RF carrier which is transmitted by the AP. The RF carrier modulation is achieved by connecting an antenna to different loads which fundamentally translates into different antenna-load reflection coefficients. Many research papers in the recent past have been presented to show fruitful applications and advantages of backscatter communications.

In recent papers [22]–[24], we developed a comprehensive framework to characterize the performance of drone-assisted backscatter and millimeter-wave simultaneous wireless information and power transfer (SWIPT) communication-based IoT

sensor networks. We considered such a scenario where a drone transmits an RF carrier which is modulated by IoT SNs and quantified the coverage probability for a single onboard SN antenna. The authors in [25], under drone energy constraints, evaluated the system average outage probability and then used the golden section method to improve the energy efficiency as well as finding the optimal backscattering drone position. Their analytical and simulation findings demonstrated that there is a compromise between the placement of the data-gathering drone location and the outage probability. In [26], the authors presented the basic principles of ambient backscatter communication (AmBC), and they analyzed its features and advantages and suggested some open issues to predict its potential applications for future IoT infrastructure. In [27], the authors introduced a 5.8-GHz backscatter tag that harnesses the quantum tunneling effect and presented their advantages in increasing the range of backscatter radio links. To increase the reliability of intelligent and passive communications, the authors in [28] introduced the idea of large intelligent surface (LIS) aided backscatter communication systems. They showed that the LIS aided backscatter can significantly impact the bit error rate performance. The idea of massive wireless energy transfer has been presented in [29]. The authors over-viewed the main architectures, challenges and techniques for efficient and salable wireless power transfer that can be considered as a key enabler of the backscatter SWIPT technology in the future of the sixth generation (6G) communications. In order to harness the backscatter technologies in the future 6G communications for vehicular to everything (V2X) scenarios, the authors in [30] presented a novel analysis for non-orthogonal multiple access (NOMA)-enabled backscatter-based V2X networks. They introduced the idea of backscattering via roadside units by applying the NOMA technique to increase the performance of the network.

Given the advantages of drone-assisted backscatter communications and its expected effect in enhancing the communication network conditions and decreasing the needed resources for the network operation, we introduce the effect of using multiple antenna backscatter tags on the performance of the overall network.

A. Contributions

The key contributions of this paper are as follows:

1) Considering a multiple antenna backscatter sensor network, we first derive the statistical characteristics of the dyadic fading channels and then employ it to study the coverage probability for a certain network geometry under a realistic path-loss model.
2) We then present an analytical framework to quantify the moments of the received signal at the reader side of the backscatter link.
3) The cumulative distribution function (CDF) of the end-to-end fading channel is quantified using higher-order moments in conjunction with the Gil-Pelaez theorem. However, this requires complex integration for which numerical integration takes a long time to converge. We present a solution based on the moments method on approximating the fading channel CDF by a Log-Normal distribution which simplifies and speeds up the evaluation of the coverage probability. Then we evaluate the convergence of the approximation in the results section.
4) We investigate the design space of the considered network and present several important insights on engineering the backscatter sensor SN network.

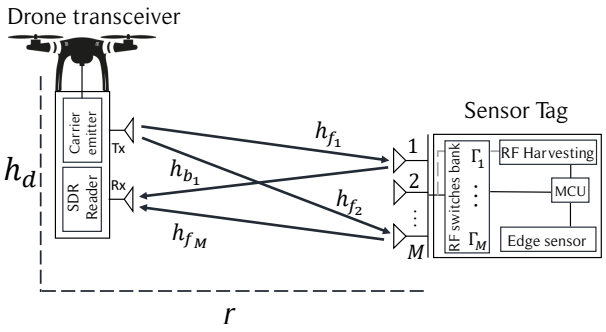

Fig. 1: System model.

B. Organization

The rest of the paper is organized as follows: Section II introduces the system model and deployment geometry of the network. Section III gives the performance analysis and mathematical modelling. Section IV presents numerical results. Finally, Section V provides some future work and conclusions.

II. SYSTEM MODEL

As shown in Fig. 1, the system model consists of a bi-static drone signal transmitter and a receiver. The transmitter emits a pure sinusoidal signal to the intended multiple antenna backscatter tag with M antennas. The antennas of the backscatter tag passively reflects the received signal after modulating the pure carrier with the sensor's data through controlling the antenna reflection factor Γ_i following the binary data of the sensor[1]. The channels from the reader to the tag and back to the drone reader are all modelled as a complex Gaussian random variables. The fading channels from the carrier emitter to the tag antennas are denoted by the symbol $\mathbf{H}_f \in \mathbb{C}^{1\times M}$ which represents the forward channel vector from the emitter to the tag such that $\mathbf{H}_f = \{h_{f_1}, ..., h_{f_M}\}$. $\mathbf{H}_b \in \mathbb{C}^{M\times 1}$ is the backward channel vector from the tag to the reader such that $\mathbf{H}_b = \{h_{b_1}, ..., h_{b_M}\}$. The dyadic channel (i.e., the cascaded channel) then can be written as the complex multiplication of the forward and the backward channel as

[1]For simplicity and without any loss of generality, we will assume that Γ_i is 1 for all the backscatter tag antennas and also the separation between the antennas is sufficient to assure independent and uncorrelated dyadic fading channels.

$\mathcal{H}_i = h_{f_i} h_{b_i}$. Hence, the overall received signal from the M dyadic channels at the reader antenna can be written as

$$y_T(t) = \sum_{i=1}^{M} \sqrt{P_t} |\mathcal{H}_i| L^{-1}(h_d, r) G(h_d, r) x(t) + n(t), \quad (1)$$

where, P_t is the transmit power, $L(h_d, r)$ is the overall path-loss for the dyadic link, $G(h_d, r)$ is the antenna gain which is dependent on the location of the backscatter tag and will be discussed later, $x(t)$ is the message signal from the tag at time t and $n(t)$ is the additive white Gaussian noise (AWGN) at the receiver. Here, we assume that the backscatter tag adds no AWGN to the reflected signal since the reflection is made without any internal processing for the pure carrier.

$$\gamma_T = \sum_{i=1}^{M} |\mathcal{H}_i|^2. \quad (2)$$

Before presenting the statistical model of γ_T, we present the link budget from the large-scale fading and the antenna point of view in the next two subsections and then later the small-scale fading.

A. Large-Scale Fading Model:

In order to accurately capture the propagation conditions for drone assisted backscatter communication, we employ the path-loss model presented in [31], [32]. The backscatter communication link is dyadic in nature, (i.e., it is characterized by the product of forward and backward channel gains). We assume that both forward and backward channels experience the same path-loss, which is reasonable for the mono-static architecture. The employed path-loss model adequately captures LoS and NLoS contributions for drone-to-ground communication as follows[2]:

$$L_L(h_d, r) = K \left(r^2 + h_{\mathrm{d}}^2 \right), \quad (3)$$

$$L_{\mathrm{NL}}(h_{\mathrm{d}}, r) = K_{\mathrm{NL}} \left(r^2 + h_{\mathrm{d}}^2 \right), \quad (4)$$

where h_{d} is the height of the drone in meters, r is the two dimensional projection separation between the drone and the SN, K_{L} and K_{NL} are environment and frequency dependent parameters such that $K_{\mathrm{i}} = \zeta_{\mathrm{i}} \left(c/(4\pi f_{\mathrm{MHz}}) \right)^{-1}$, ζ_{i} is the excess path-loss for $i \in \{L, NL\}$ with typical values for urban areas $\zeta_{\mathrm{LoS}} = 1$ dB. The probabilities of having a LoS and NLoS link between the DFR and the desired SN are as follows:

$$\mathcal{P}_{\mathrm{L}}(h_{\mathrm{d}}, r) = \frac{1}{1 + a\, \mathrm{e}^{-b\eta \tan^{-1}\left(\frac{r}{h_{\mathrm{d}}}\right) + b\, a}}, \quad (5a)$$

$$\mathcal{P}_{\mathrm{NL}}(h_{\mathrm{d}}, r) = 1 - \mathcal{P}_{\mathrm{L}}(h_{\mathrm{d}}, r), \quad (5b)$$

where a, b, c are environment dependent constants and $\eta = 180/\pi$.

[2]From now on, we will write the subscripts L and NL to refer to LoS and $NLoS$, respectively.

B. Antenna gain

In order to reflect the effect of the drone antenna gain pattern, we use a simple elliptical approximation of the antenna gain pattern at which we will only have a main lobe with varying gains according to the elevation angle of the drone to the backscatter tag. As the elevation angle ϕ_e is a function of the drone height and the tag horizontal distance, we can write the antenna power gain factor as

$$G(h_d, r) = A \cos^{\mathcal{K}} \left(\frac{\pi}{2} - \phi_e \right) = A \cos^{\mathcal{K}} \left(\frac{\pi}{2} - \tan^{-1} \left(\frac{h_d}{r} \right) \right), \quad (6)$$

where A is the power gain of the antenna at distance $r = 0$ (i.e., $\phi_e = \frac{\pi}{2}$) and $\mathcal{K}$ is a factor that determines the antenna gain main lobe width where $\mathcal{K}$ is any positive number. Increasing the factor $\mathcal{K}$ makes the antenna more directional.

C. Small-Scale Dyadic Rayleigh Fading Channel

As we already mentioned, the small-scale fading channel is a dyadic channel where the channel model is the product of two complex Gaussian fading channels. Hence, the envelope of the one hop fading channel (i.e., the forward or the backward channels) follows the Rayleigh distribution. The dyadic $\mathcal{H}$ channel is usually modeled in the literature as the product of two correlated fading channels with a correlation factor ρ where the channel envelope $\mathcal{H}$ follows the envelope of the transformation of the two complex channels h_f and h_b. So, we can write $\mathcal{H} = |h_f h_b|$, where $h_b = \rho h_f + \sqrt{1-\rho^2} h_b^*$ and h_b^* is the backward independent Rayleigh fading channel coefficient as an intermediate step in finding the correlated dyadic fading channel coefficient $\mathcal{H}$. The PDF of $\mathcal{H}$ can be written as both forward and backward Rayleigh channels with unit mean, (i.e., $\mathbb{E}(h_{\mathrm{f}}) = \mathbb{E}(h_{\mathrm{b}}) = 1$):

$$f_{\mathcal{H}}(h) = \frac{4y}{1-\rho^2} I_0 \left(2\, \frac{\rho\, h}{1-\rho^2} \right) K_0 \left(2\, \frac{h}{1-\rho^2} \right). \quad (7)$$

In this article, for the sake of simplicity and tractability, we will assume only uncorrelated backscatter channels. For $\rho = 0$, which means that the forward and the backward link are not correlated, we can write the PDF of the channel envelope as

$$f_{\mathcal{H}}(h) = 4y\, K_0\,(2\, h), \quad (8)$$

where $K_o(z) = \int_0^\infty \cos(z \sinh(t))\, \mathrm{d}t$, is the modified Bessel function of second kind and zero-order. This shape of the dyadic fading channel is also known in the literature as the double-Rayleigh fading channel. Doing a simple random variable transformation to compute the distribution of the fading channel power such that $\gamma = \mathcal{H}^2$ results in the PDF of γ as

$$f_{\gamma = \mathcal{H}^2}(\gamma) = 2\, K_0 \left(2\, \sqrt{\gamma} \right). \quad (9)$$

The nth moment of the fading channel envelope can be found by averaging the PDF of $\mathcal{H}$ and can be written as

$$\mathbb{E}_{\mathcal{H}} \left[\mathcal{H}^n \right] = \left(\Gamma \left(1 + n/2 \right) \right)^2, \quad (10)$$

where $\Gamma(z) = \int_0^\infty x^{z-1}e^{-x}\,dx$ is the Gamma function. Also, the nth moment of the channel fading power can be evaluated as

$$\mathbb{E}_{\gamma^2}\left[\gamma^n\right] = \left(\Gamma\left(1+n\right)\right)^2. \tag{11}$$

Given the statistical characteristics of the dyadic fading channel, we now move to the performance analysis.

III. Performance analysis

A. Coverage Probability

The coverage probability is defined as the probability that the total SNR will be greater than a certain predefined value β. The SNR at the receiver for a specific location r can be divided into two terms depending upon whether the drone-to-tag link is LoS or NLoS:

$$\text{SNR}_L = \frac{P_\text{t}\gamma_T L_\text{L}^{-2}(h_d,r)G^2(h_d,r)}{\sigma_\text{N}^2}, \tag{12}$$

$$\text{SNR}_{NL} = \frac{P_\text{t}\gamma_T L_\text{NL}^{-2}(h_d,r)G^2(h_d,r)}{\sigma_\text{N}^2}, \tag{13}$$

where P_t is the reader's transmit power, σ_N^2 is the additive white Gaussian noise (AWGN) power, SNR_L is the SNR when there is a LoS link between the user and the BS and SNR_NL is the SNR when there is a NLoS link between the user and the drone flying reader (DFR). Hence, the coverage probability for any arbitrary mobile user can be evaluated as

$$\begin{aligned} P_c &= \Pr[\text{SNR}_L \geq \beta] \times \mathcal{P}_\text{L}(h_\text{d},r) \\ &\quad + \Pr[\text{SNR}_{NL} \geq \beta] \times \mathcal{P}_\text{NL}(h_\text{d},r). \end{aligned} \tag{14}$$

The evaluation of P_c requires the evaluation of the two values

$$\Pr[\text{SNR}_L \geq \beta] = \Pr\left\{\gamma_T \geq \underbrace{\frac{\beta\sigma_\text{N}^2 L_\text{L}^2(h_d,r)}{P_\text{t}G^2(h_d,r)}}_{\beta_L}\right\}, \tag{15}$$

$$\Pr[\text{SNR}_{NL} \geq \beta] = \Pr\left\{\gamma_T \geq \underbrace{\frac{\beta\sigma_\text{N}^2 L_\text{NL}^2(h_d,r)}{P_\text{t}G^2(h_d,r)}}_{\beta NL}\right\}, \tag{16}$$

where $\Pr\{\gamma_T \geq \xi\}$ can be seen as the complementary CDF (CCDF) of γ_T (i.e., $1 - F_{\gamma_T}(\xi)$). However, we do not have any close form expression for the CCDF of the overall received signal γ_T which is the summation of the power of the identically independent distributions (i.i.d) $\mathcal{H}_i$. However, the calculation of the CCDF is made possible using the CDF inversion theorem using the Gil-Pelaez theorem [33] and hence the CDF of γ_T at any given point ξ can be written as

$$F_{\gamma_T}(\xi) = \frac{1}{2} + \frac{1}{\pi}\int_0^\infty \frac{\text{Im}[e^{-jt\xi}\varphi_{\gamma_T}(\xi)]}{t}\,\text{d}t, \tag{17}$$

where $\varphi_{\gamma_T}(\xi)$ is the characteristic function of γ_T evaluated at any arbitrary point ξ at the support of γ_T. The characteristic function of γ can be written as

$$\varphi_\gamma(s) = \frac{j}{s}\exp\left(\frac{j}{s}\right)E_i\left(\frac{j}{s}\right). \tag{18}$$

where $E_i(x) = -\int_{-x}^\infty \frac{e^{-t}}{t}\,dt$ is the the exponential integral. Hence, the total received power at the end of the multi antenna dyadic channel (i.e., the reader's antenna) has the characteristic function:

$$\varphi_{\alpha_T}(s) = \left(\frac{j}{s}\exp\left(\frac{j}{s}\right)E_i\left(\frac{j}{s}\right)\right)^M, \tag{19}$$

Given the characteristic function of the received power, we can use the Gil-Pelaez theorem of CDF inversion to compute $F_{\gamma_T}(\xi)$. Therefore, (14) can be written as

$$\begin{aligned} P_c &= [1 - F_{\gamma_T}(\beta_L)] \times \mathcal{P}_\text{L}(h_\text{d},r) \\ &\quad + [1 - F_{\gamma_T}(\beta_{NL})] \times \mathcal{P}_\text{NL}(h_\text{d},r). \end{aligned} \tag{20}$$

Noting that the evaluation of the coverage probability using the Gil-Pelaez theorem involves the computation of multiple folded integrals, and we will use the method of moments to find a good match for $F_{\gamma_T}(\xi)$ in the following subsection.

B. Method of Moments for PDF Matching

In statistics, the method of moments is widely used to approximate or estimate the random variable distribution (i.e., PDF and CDF). The idea of the moment matching is to fit the moments of the sum of the received signal on the receiver's (γ_T) side to a well-known PDF. In the literature, the Log-Normal distribution has been successful in matching the PDF of the sum of i.i.d random variables with a good fitness. The PDF and the CDF of the Log-Normal distribution are

$$\text{PDF}: \quad f_X(x) = \frac{1}{x\sigma\sqrt{2\pi}}\exp\left(-\frac{(\ln x - \mu)^2}{2\sigma^2}\right), \tag{21}$$

$$\text{CDF}: \quad F_X(x) = \frac{1}{2} + \frac{1}{2}\,\text{erf}\left(\frac{\ln x - \mu}{\sqrt{2}\sigma}\right), \tag{22}$$

where μ and σ are respectively the expected value and standard deviation of the natural logarithm of the random variable X. The idea of the moments matching is to find the values of μ and σ from the first moment and the variance of γ_T (i.e., $\mathbb{E}[\gamma_T]$ and $\mathbb{E}[(\gamma_T - \mathbb{E}[\gamma_T])^2] = \text{Var}(\gamma_T)$). Therefore, matching the random variable γ_T involves finding the values of μ and σ which can be written as

$$\mu_{\gamma_T} = \ln\left(\frac{\mathbb{E}[\gamma_T]^2}{\sqrt{\text{Var}(\gamma_T) - \mathbb{E}[\gamma_T]^2}}\right), \tag{23}$$

$$\sigma_{\gamma_T} = \sqrt{\ln\left(\frac{\text{Var}(\gamma_T)}{\mathbb{E}[\gamma_T]^2} + 1\right)}. \tag{24}$$

Given the values of μ_{γ_T} and σ_{γ_T}, the PDF and CDF of γ_T can be approximated as

$$\text{PDF}: \; f_{\gamma_T}(x) \sim \frac{1}{x\sigma_{\gamma_T}\sqrt{2\pi}}\exp\left(-\frac{(\ln x - \mu_{\gamma_T})^2}{2\sigma_{\gamma_T}^2}\right), \tag{25}$$

$$\text{CDF}: \; F_{\gamma_T}(x) \sim \frac{1}{2} + \frac{1}{2}\,\text{erf}\left(\frac{\ln x - \mu_{\gamma_T}}{\sqrt{2}\sigma_{\gamma_T}}\right). \tag{26}$$

Computation of the Kullback-Leibler (KL) divergence is a well known method to quantify the difference between the PDF of two random variables. However, we will examine the convergence of the approximation in the results section through comparing it by the exact and Monte-Carlo simulations. Unfortunately, we cannot find the value of the second moment of γ_T directly from the characteristic function since it does not exist due as the derivative of the characteristic function of γ_T does not exist for the value $s = 0$. Hence, the characteristic function cannot be used to derive the second moment of γ_T. Thus, we use the second derivative of the moment generation function $\mathcal{M}_{\gamma_T}(t) = \varphi(-it)$ and hence the first moment and the variance of γ_T moment can be written as shown in the following proposition.

Proposition 1. *The first moment and the variance of the random variable γ_T can be evaluated as*

$$\mathbb{E}[\gamma_T] = M, \tag{27}$$

$$\sigma^2_{\gamma_T} = \mathbb{E}[(\gamma_T - \mathbb{E}[\gamma_T])^2] = M^2 + 3M. \tag{28}$$

Proof. The derivation of the first two moments is easy and follows transforming the characteristic function by simply applying $\mathcal{M}_{\gamma_T}(s) = \varphi_{\gamma_T}(-is)$ to find the MGF of γ_T that can be written as

$$\mathcal{M}_{\gamma_T}(s) = \left(-\frac{1}{s} \exp\left(\frac{-1}{s}\right) E_i\left(\frac{-1}{s}\right) \right)^M. \tag{29}$$

Then, we find the nth moment $\mathbb{E}_{\gamma_T}[\gamma_T]$ as

$$\mathbb{E}\left(\gamma_T^n\right) = \mathcal{M}^{(n)}_{\gamma_T}(0) = \left. \frac{d^n \mathcal{M}_{\gamma_T}(s)}{dt^n} \right|_{s=0}. \tag{30}$$

Then, given the two derivatives of the MGF and finding the limits $\lim_{s\to 0} \frac{d\mathcal{M}_{\gamma_T}(s)}{dt}$ and $\lim_{s\to 0} \frac{d^2\mathcal{M}_{\gamma_T}(s)}{dt^2}$ and knowing that $\sigma^2_{\gamma_T} = \mathbb{E}\left(\gamma_T^2\right) - \mathbb{E}\left(\gamma_T\right)^2$, we can write (27) and (28). Please note however, that the first moment of γ_T could be evaluated simply by relying on the assumption that the sum of M i.i.d random variables is simply the sum of their expectations which follows from the value in (11) with $N = 1$ which gives 1 and this validates the evaluation of (27) using the MGF approach. □

Substituting (27) and (28) into (23) and (24) we can write

$$\mu_{\gamma_T} = \ln\left(\frac{M}{\sqrt{M\left(M+3\right)}}\right), \sigma_{\gamma_T} = \sqrt{\ln\left(\frac{3}{M}+1\right)}. \tag{31}$$

Then plugging the values in (31) in (26) and then (26) in (20) will give us the approximate coverage probability for the overall link.

IV. Numerical Results

In this section, we validate the developed statistical framework for quantifying the coverage probability. We also briefly explore the impact of different parametric variations on the coverage probability. We assume an urban environment with the parameters $a = 9.6$, $b = 0.28$ for the path-loss model, noise power σ^2_N = - 55 dBm, $P_t = 0$ dB and $f = 1000$ MHz carrier emitter frequency. Also, as described in the previous sections, we consider uncorrelated Rayleigh flat wireless dyadic fading channels. The noise power is estimated from the practical implementations.

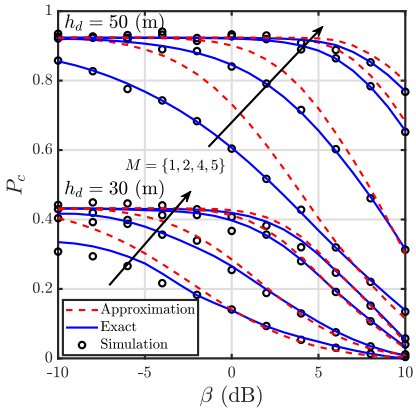

Fig. 2: Coverage probability with $r = 100$ (m) and $\sigma^2_N = -55$ dBm.

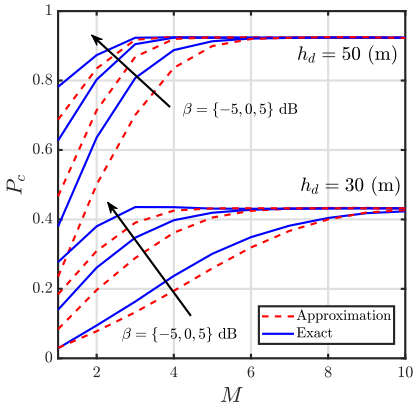

Fig. 3: Coverage probability with $r = 100$ (m) and $\sigma^2_N = -55$ dBm.

1) Fitness of the Log-Normal Approximation: Fig. 2 shows the coverage probability against the threshold value β. The figure presents a comparison between the exact closed-form expression as presented in (20), the Log-Normal approximation as measured by applying the CDF in (26) and the Monte-Carlo simulations. The figure shows a very good fit for the Log-Normal approximation, especially for the higher number of the antennas on the backscatter. For example, the curve for the setup with $h_d = 50$ (m) for $M = 5$ shows a very close fit even for the low values of the coverage threshold β. The figure also dictates the effect of changing the drone height on the overall coverage probability. For example, a drone height of 50 (m) results on higher coverage when compared to 30 (m). The result is due to the effect of the antenna gain pattern

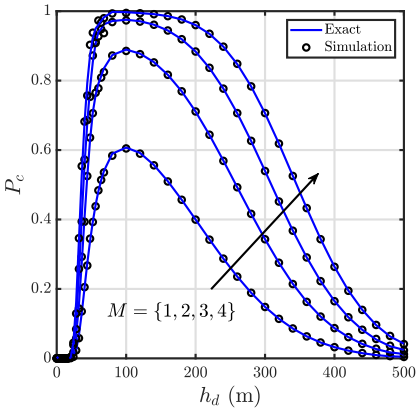

Fig. 4: Coverage probability with $r = 100$ (m), $\sigma_N^2 = -55$ dBm and $\beta = 5$ dB.

and the increase of the probability of LoS links between the drone and the SN.

Fig. 3 studies the effect of increasing the number of tag antennas on the overall coverage probability at different setups. The figure shows a very high precision of the approximation as the number M increases. In particular, the figure shows that a coverage match accrues as the number of antennas M goes beyond five antennas for most of the setups and for different values of the coverage probability threshold β. The figure also shows that the same number M reflects the number at which the fitness of the approximation becomes very precise. This is intuitive, due to the fact that the Log-Normal distribution is in fact a Normal distribution but then it is transformed into a log scale.

2) Optimal Trajectory and Antenna Gain Pattern Effect: Fig. 4 presents the coverage probability against the drone height (h_d). It is very clear from the figure that there is always an optimal height for the drone at which the coverage probability starts to decrease. Again, this is due to the increase of the LoS probability which increases to some point and then starts to reduce. Increasing the probability of LoS increases the coverage probability to the point where the path-loss will be dominant on the LoS link favorable conditions and the advantages of increasing the height of the drone starts to vanish and the coverage probability will start to decrease. It also shows the effect of increasing the number of antennas on the overall coverage probability. Again, increasing the number of antennas on the backscatter tag increases the coverage probability. However, the advantages of increasing the number of antennas (i.e., the diversity gain) are larger when increasing the number of antennas from one to two. It is also worth mentioning that the number of antennas of the tag does not affect the optimal height of the drone. This is intuitive since the number of antennas is not related to the distances and the channel conditions. However, one may argue that the location of the antennas is essential in determining the channel conditions. In this paper, we assume that the trajectory distances of the drone and the SN tag are large enough to neglect the antennas separation, and also the elevation angles of all of the antennas to the drone's transmitter and receiver are the same.

V. Conclusion

In this paper, we investigated the idea of drone-assisted multiple antenna backscatter communications. We developed a point-to-point implementation of the multiple antenna system involving the channel conditions of the framework. In particular, our model explicitly incorporates a dyadic fading channel where the forward (Drone-to-SN) and backward (SN-to-Drone) propagation channels are uncorrelated Rayleigh fading channels which results in a double Rayleigh dyadic channel. Performance analysis for the dyadic multiple antenna links is performed using multiple closed-form expressions. The developed model is examined using the characteristic function and moment generation function methods. We also use the CDF inversion theorem and subsequently supported by a CDF approximation using the method of moments to evaluate the PDF of the received power of the multiple antenna channel. We demonstrate that there exists a fruitful interplay between the SN's antennas number, drone height, and antenna gain patterns which jointly dictates an optimal operation point at which coverage probability is maximized.

Acknowledgement

This work was supported by the Royal Academy of Engineering grant Transforming Systems through Partnership TSP1040. Part of this project was supported by the Royal Academy through the Distinguished International Associates grant, DIA-2021-18 and the ASPIRE Award for Research Excellence Program 2020 (Abu Dhabi, UAE) under grant AARE20–161.

References

[1] R. Halloush, H. B. Salameh, A. Musa, M. Halloush, and M. A. Shunnar, "Highly-reliable transmission and channel assignment for cr-iot networks," *IEEE Internet of Things Journal*, pp. 1–1, 2021.

[2] H. A. B. Salameh, M. Bani Irshaid, A. Al Ajlouni, and M. Aloqaily, "Energy-efficient cross-layer spectrum sharing in cr green iot networks," *IEEE Transactions on Green Communications and Networking*, vol. 5, no. 3, pp. 1091–1100, 2021.

[3] H. Hui, Y. Ding, Q. Shi, F. Li, Y. Song, and J. Yan, "5g network-based internet of things for demand response in smart grid: A survey on application potential," *Applied Energy*, vol. 257, p. 113972, 2020.

[4] H. Shakhatreh, A. Khreishah, J. Chakareski, H. B. Salameh, and I. Khalil, "On the continuous coverage problem for a swarm of uavs," in *2016 IEEE 37th Sarnoff Symposium*, pp. 130–135, 2016.

[5] A. M. Hayajneh, S. A. R. Zaidi, D. C. McLernon, M. Di Renzo, and M. Ghogho, "Performance analysis of uav enabled disaster recovery networks: A stochastic geometric framework based on cluster processes," *IEEE Access*, vol. 6, pp. 26215–26230, 2018.

[6] A. M. Hayajneh, S. A. R. Zaidi, D. C. McLernon, and M. Ghogho, "Drone empowered small cellular disaster recovery networks for resilient smart cities," in *2016 IEEE international conference on sensing, communication and networking (SECON Workshops)*, pp. 1–6, IEEE, 2016.

[7] A. M. Hayajneh, S. A. R. Zaidi, D. C. McLernon, and M. Ghogho, "Optimal dimensioning and performance analysis of drone-based wireless communications," in *2016 IEEE Globecom Workshops (GC Wkshps)*, pp. 1–6, IEEE, 2016.

[8] N. Zhao, W. Lu, M. Sheng, Y. Chen, J. Tang, F. R. Yu, and K.-K. Wong, "Uav-assisted emergency networks in disasters," *IEEE Wireless Communications*, vol. 26, no. 1, pp. 45–51, 2019.

[9] S. Chandrasekharan, K. Gomez, A. Al-Hourani, S. Kandeepan, T. Rasheed, L. Goratti, L. Reynaud, D. Grace, I. Bucaille, T. Wirth, *et al.*, "Designing and implementing future aerial communication networks," *IEEE Communications Magazine*, vol. 54, no. 5, pp. 26–34, 2016.

[10] M. Mozaffari, W. Saad, M. Bennis, Y.-H. Nam, and M. Debbah, "A tutorial on uavs for wireless networks: Applications, challenges, and open problems," *IEEE communications surveys & tutorials*, vol. 21, no. 3, pp. 2334–2360, 2019.

[11] O. Bouachir, M. Aloqaily, I. A. Ridhawi, O. Alfandi, and H. B. Salameh, "Uav-assisted vehicular communication for densely crowded environments," in *NOMS 2020 - 2020 IEEE/IFIP Network Operations and Management Symposium*, pp. 1–4, 2020.

[12] V. Liu, A. Parks, V. Talla, S. Gollakota, D. Wetherall, and J. R. Smith, "Ambient backscatter: wireless communication out of thin air," in *ACM SIGCOMM Computer Communication Review*, vol. 43, pp. 39–50, ACM, 2013.

[13] A. Bletsas, P. N. Alevizos, and G. Vougioukas, "The art of signal processing in backscatter radio for μw (or less) internet of things: Intelligent signal processing and backscatter radio enabling batteryless connectivity," *IEEE Signal Processing Magazine*, vol. 35, no. 5, pp. 28–40, 2018.

[14] E. Kampianakis, J. Kimionis, K. Tountas, C. Konstantopoulos, E. Koutroulis, and A. Bletsas, "Wireless environmental sensor networking with analog scatter radio and timer principles," *IEEE Sensors Journal*, vol. 14, no. 10, pp. 3365–3376, 2014.

[15] C. Xu, L. Yang, and P. Zhang, "Practical backscatter communication systems for battery-free internet of things: A tutorial and survey of recent research," *IEEE Signal Processing Magazine*, vol. 35, no. 5, pp. 16–27, 2018.

[16] N. Van Huynh, D. T. Hoang, X. Lu, D. Niyato, P. Wang, and D. I. Kim, "Ambient backscatter communications: A contemporary survey," *IEEE Communications surveys & tutorials*, vol. 20, no. 4, pp. 2889–2922, 2018.

[17] F. Jameel, R. Duan, Z. Chang, A. Liljemark, T. Ristaniemi, and R. Jantti, "Applications of backscatter communications for healthcare networks," *IEEE Network*, vol. 33, no. 6, pp. 50–57, 2019.

[18] R. Long, H. Guo, L. Zhang, and Y.-C. Liang, "Full-duplex backscatter communications in symbiotic radio systems," *IEEE Access*, vol. 7, pp. 21597–21608, 2019.

[19] R. Duan, X. Wang, H. Yigitler, M. U. Sheikh, R. Jantti, and Z. Han, "Ambient backscatter communications for future ultra-low-power machine type communications: Challenges, solutions, opportunities, and future research trends," *IEEE Communications Magazine*, vol. 58, no. 2, pp. 42–47, 2020.

[20] H. B. Salameh, R. Tashtoush, H. Al-Obiedollah, A. Alajlouni, and Y. Jararweh, "Power allocation technique with soft performance guarantees in hybrid ofdma–noma cognitive radio systems: Modeling and simulation," *Simulation Modelling Practice and Theory*, vol. 112, p. 102370, 2021.

[21] H. Al-Obiedollah, K. Cumanan, H. B. Salameh, G. Chen, Z. Ding, and O. A. Dobre, "Downlink multi-carrier noma with opportunistic bandwidth allocations," *IEEE Wireless Communications Letters*, 2021.

[22] A. Hayajneh, S. A. R. Zaidi, M. Hafeez, D. McLernon, and M. Win, "Coverage analysis of drone-assisted backscatter communication for iot sensor network," in *2019 15th International Conference on Distributed Computing in Sensor Systems (DCOSS)*, pp. 584–590, IEEE, 2019.

[23] S. A. R. Zaidi, M. Hafeez, D. McLernon, and M. Z. Win, "Coverage analysis for backscatter communication empowered cellular internet-of-things," in *2019 27th European Signal Processing Conference (EUSIPCO)*, pp. 1–5, IEEE, 2019.

[24] B. T. Malik, V. Doychinov, A. M. Hayajneh, S. A. R. Zaidi, I. D. Robertson, and N. Somjit, "Wireless power transfer system for battery-less sensor nodes," *IEEE Access*, vol. 8, pp. 95878–95887, 2020.

[25] S. Yang, Y. Deng, X. Tang, Y. Ding, and J. Zhou, "Energy efficiency optimization for uav-assisted backscatter communications," *IEEE Communications Letters*, vol. 23, no. 11, pp. 2041–2045, 2019.

[26] W. Zhang, Y. Qin, W. Zhao, M. Jia, Q. Liu, R. He, and B. Ai, "A green paradigm for internet of things: Ambient backscatter communications," *China Communications*, vol. 16, no. 7, pp. 109–119, 2019.

[27] F. Amato, H. M. Torun, and G. D. Durgin, "Rfid backscattering in long-range scenarios," *IEEE Transactions on Wireless Communications*, vol. 17, no. 4, pp. 2718–2725, 2018.

[28] W. Zhao, G. Wang, S. Atapattu, T. A. Tsiftsis, and X. Ma, "Performance analysis of large intelligent surface aided backscatter communication systems," *IEEE Wireless Communications Letters*, vol. 9, no. 7, pp. 962–966, 2020.

[29] O. L. López, H. Alves, R. D. Souza, S. Montejo-Sánchez, E. M. G. Fernández, and M. Latva-Aho, "Massive wireless energy transfer: Enabling sustainable iot toward 6g era," *IEEE Internet of Things Journal*, vol. 8, no. 11, pp. 8816–8835, 2021.

[30] W. U. Khan, F. Jameel, N. Kumar, R. Jäntti, and M. Guizani, "Backscatter-enabled efficient v2x communication with non-orthogonal multiple access," *IEEE Transactions on Vehicular Technology*, vol. 70, no. 2, pp. 1724–1735, 2021.

[31] M. Mozaffari, W. Saad, M. Bennis, and M. Debbah, "Drone small cells in the clouds: Design, deployment and performance analysis," *arXiv preprint arXiv:1509.01655*, 2015.

[32] A. Al-Hourani, S. Kandeepan, and S. Lardner, "Optimal lap altitude for maximum coverage," *Wireless Communications Letters, IEEE*, vol. 3, no. 6, pp. 569–572, 2014.

[33] J. Gil-Pelaez, "Note on the inversion theorem," *Biometrika*, vol. 38, no. 3-4, pp. 481–482, 1951.